


Article

Processing–Microstructure Relation of Deformed and Partitioned (D&P) Steels

Li Liu ^{1,2}, Binbin He ^{1,2} and Mingxin Huang ^{1,2,*} 

¹ Department of Mechanical Engineering, The University of Hong Kong, Hong Kong 999077, China; liliu@hku.hk (L.L.); hebinbin@hku.hk (B.H.)

² Shenzhen Institute of Research and Innovation, The University of Hong Kong, Shenzhen 518057, China

* Correspondence: mxhuang@hku.hk; Tel.: +852-28597906; Fax: +852-28585415

Received: 22 May 2019; Accepted: 19 June 2019; Published: 20 June 2019



Abstract: An ultrastrong and ductile deformed and partitioned (D&P) steel developed by dislocation engineering has been reported recently. However, the microstructure evolution during the D&P processes has not yet been fully understood. The present paper aims to elucidate the process–microstructure relation in D&P process. Specifically, the evolution of phase fraction and microstructure during the corresponding D&P process are captured by means of X-ray diffraction (XRD) and electron backscatter diffraction (EBSD). Subsequently, the effect of partitioning temperature on dislocation density and mechanical properties of D&P steel is investigated with the assistance of uniaxial tensile tests and synchrotron X-ray diffraction. It is found that a heterogeneous microstructure is firstly realized by hot rolling. The warm rolling is crucial in introducing dislocations, while deformation-induced martensite is mainly formed during cold rolling. The dislocation density of the D&P steel gradually decreases with the increase of partitioning temperature, while the high yield strength is maintained owing to the bake hardening. The ductility is firstly enhanced while then deteriorated by increasing partitioning temperature due to the strong interaction between dislocation and interstitial atoms at higher partitioning temperatures.

Keywords: D&P steel; processing; microstructure; phase transformation; dislocation density; mechanical properties

1. Introduction

Strong and ductile metallic materials are ideal to develop high-performance yet energy-efficient structural components for many applications [1,2]. Unfortunately, strength and ductility are, in general, mutually exclusive in metallic materials [3,4]. Sustained effort has been paid to overcome the strength–ductility trade-off of structural materials. Alloying by the addition of cobalt and titanium is an effective way to simultaneously improve the strength and ductility. Nevertheless, this strategy is not cost-efficient for the industrial application and not sustainable for the limited resources on earth [5]. Developing novel thermal-mechanical process to tune the microstructure is an alternative way to resolve such trade-off. For example, quenching and partitioning (Q&P) treatment enables a dual-phase microstructure of retained austenite embedded and martensite matrix has been successfully applied to medium Mn steel, austenitic stainless steel, and martensitic stainless steel [6–8]. The retained austenite can provide transformation-induced plasticity (TRIP) effect to improve strain hardening rate, delaying the onset of necking and leading to the high strength and good ductility [9]. Recently, a novel dislocation engineering concept was employed to introduce intensive dislocations in a deformed and partitioned (D&P) steel that achieves an ultrahigh yield strength (~2.2 GPa) without compromising ductility (uniform elongation is up to ~16%) [10]. In general, strength tends to increase as dislocation density increases by resisting dislocation motion. However, ductility, which requires the glide of

dislocations, is deteriorated by abundant dislocations [11]. Opposite to such traditional view, the D&P steel demonstrates that a high dislocation density can simultaneously introduce ultrahigh yield strength as well large ductility [10]. The D&P steel shows a dual-phase heterogeneous microstructure with metastable retained austenite embedded in a highly dislocated martensitic matrix [10,12]. The retained austenite provides TRIP effect upon deformation [9]. Intensive dislocations not only provide dislocation hardening for high strength but promote ductility by glides of mobile dislocations [10,13].

The excellent mechanical properties are tailored by the corresponding D&P process. However, the evolution of microstructure during the D&P process has not yet been fully understood, which are crucial to the industrialization of the D&P steel. Meanwhile, the effect of partitioning parameters on the properties of D&P steel has not yet been discussed. Therefore, the present study investigates the contribution of different processing step of the D&P process, especially the partitioning temperature, on microstructure evolution and consequently mechanical properties of the D&P steel.

2. Materials and Methods

The investigated D&P steel has a chemical composition of Fe-10Mn-0.47C-0.7V-2Al (in wt %). Figure 1 is a schematic illustration on the thermal-mechanical processing route to produce the D&P steel. The as-received ingot is firstly homogenized at 1150 °C for 2.5 h, followed by hot rolling (HR) down to a thickness of 4 mm. The hot rolled sheet is further warm rolled (WR) at 750 °C with a total thickness reduction of 50% and is then intercritical annealed (IA) at 620 °C for 5 h. Afterwards, the sheet is further subjected to cold rolling (CR) with a thickness reduction of 30%, giving the final thickness of about 1.4 mm. The specimens subjected to HR, WR, IA, and CR are named as “Deformed” samples for brevity. Finally, Deformed samples are tempered at various temperatures for carbon partitioning from martensite to austenite to optimize austenite stability. Specimens tempered at 200 °C, 300 °C, and 400 °C are referred to D&P200, D&P300, and D&P400, respectively.

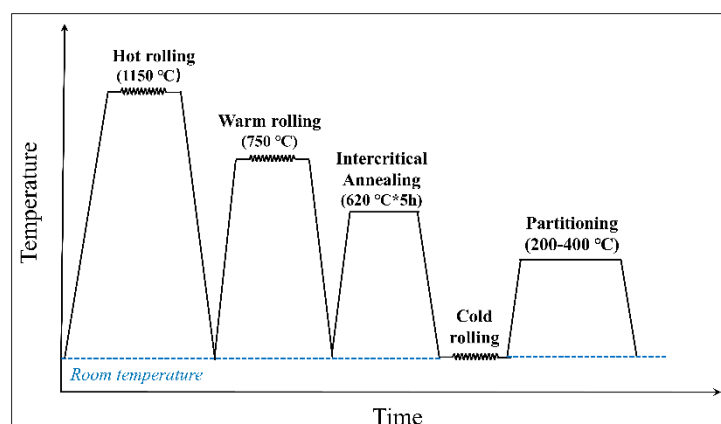


Figure 1. The schematic illustration on the thermal-mechanical processing route to produce the deformed and partitioned (D&P) steel.

The evolution of phase fraction during the whole thermomechanical process is monitored by X-ray diffraction (XRD) carried out on a Rigaku diffractometer (Rigaku Corporation, Tokyo, Japan) operating in the reflection mode with Cu K α radiation (wavelength = 1.542 Å). Scanning is performed from 40 to 100 degree at a counting rate of 0.01°·s^{−1}. Diffraction peaks including (110) α , (200) α , (211) α , (200) γ , (220) γ , and (311) γ are selected to determine the phase fraction of austenite and martensite. The cross-section along rolling direction (RD) of samples is mechanically polished down to 1 μ m followed by electrical polishing in a solution of 20% perchloric acid and 80% acetic acid (vol %) for XRD measurement and further microstructure observation. The microstructure is captured by electron backscatter diffraction (EBSD) with an LEO 1530 FEG SEM (Zeiss, Oberkochen, Germany) operated at 20 kV with a step size of 0.25 μ m. Vickers hardness measurements are conducted on the electropolished

samples with a peak load of 200 gf at ambient temperature. Dog-bone-shaped tensile specimens with a gauge length of 12 mm, thickness of 1.4 mm, and width of 4 mm are machined from the tempered sheets. Tensile tests are performed using a universal tensile testing machine under a strain rate of 10^{-3} s^{-1} at room temperature. To determine the dislocation density of the martensitic matrix of the D&P steel, synchrotron X-ray diffraction with a wavelength of 0.0688 nm, and a two-dimensional (2D) detector are performed on the electropolished samples at the BL14B beamline of Shanghai Synchrotron Radiation Facility (SSRF) (Shanghai, China). The 2D X-ray diffraction pattern is converged to intensity-2theta profiles by Fit2d for further calculation. The modified Williamson–Hall method is employed to obtain the dislocation density from the synchrotron X-ray profiles [14].

3. Results

The evolution of phase fraction during thermal-mechanical processing of the D&P steel process is demonstrated in Figure 2. The specimens had almost fully austenitic microstructure after HR and WR (Figure 2a). The volume fraction of austenite was slightly decreased after intercritical annealing, indicating that ferrite transformation is negligible during IA. This can be explained by the strong hardenability caused by high Mn content (10%) (Figure 2a). A large amount of austenite grains transformed to martensite during the subsequent cold rolling process. Around 18% of austenite was retained after cold rolling and it basically remained unchanged during subsequent partitioning process, confirming that almost no phase transformations took place during low-temperature partitioning process (Figure 2b).

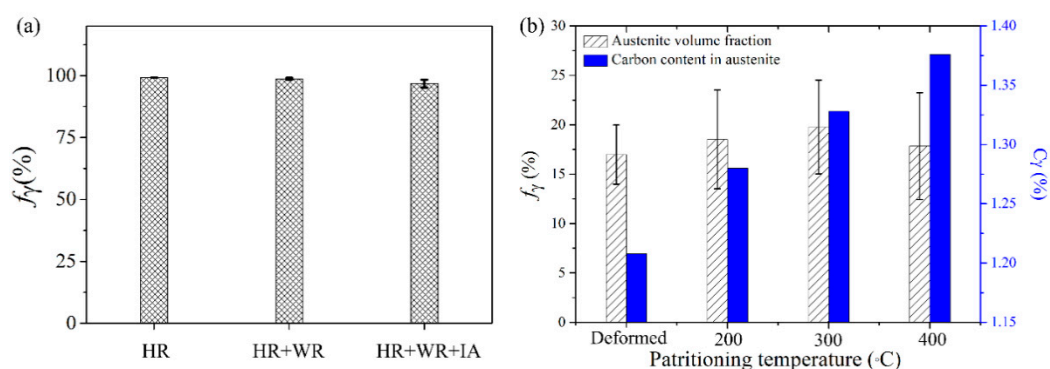


Figure 2. (a) The evolution of austenite phase fraction during HR (hot rolling), WR (warm rolling), and IA process (intercritical annealed). (b) The phase fraction and increment of carbon content of austenite in Deformed, D&P200, D&P300, and D&P400 samples.

Although the partitioning process had a less-significant effect on the austenite fraction, it influenced the carbon content and, consequently, the stability of austenite. The carbon content of austenite, which can be estimated from the peak shift of XRD profiles [15,16], was increased by 0.072, 0.12, and 0.168% after partitioning at 200, 300, and 400 °C, respectively (Figure 2b).

The typical microstructure of HR, HR + WR, and D&P specimens were characterized by EBSD, as shown in Figure 3. The HR specimen had an austenitic microstructure with prior austenite grain boundaries (PAGBs) decorated with granular submicron ferrite grains (Figure 3a1,a2). The fraction of austenite obtained from EBSD microstructure was quantitatively consistent with the XRD results. The coarse austenite grains (5–30 μm) dominated the microstructure, while some recrystallized austenite grains ($\sim 0.5 \mu\text{m}$) were found at PAGBs (Figure 3a1,a2).

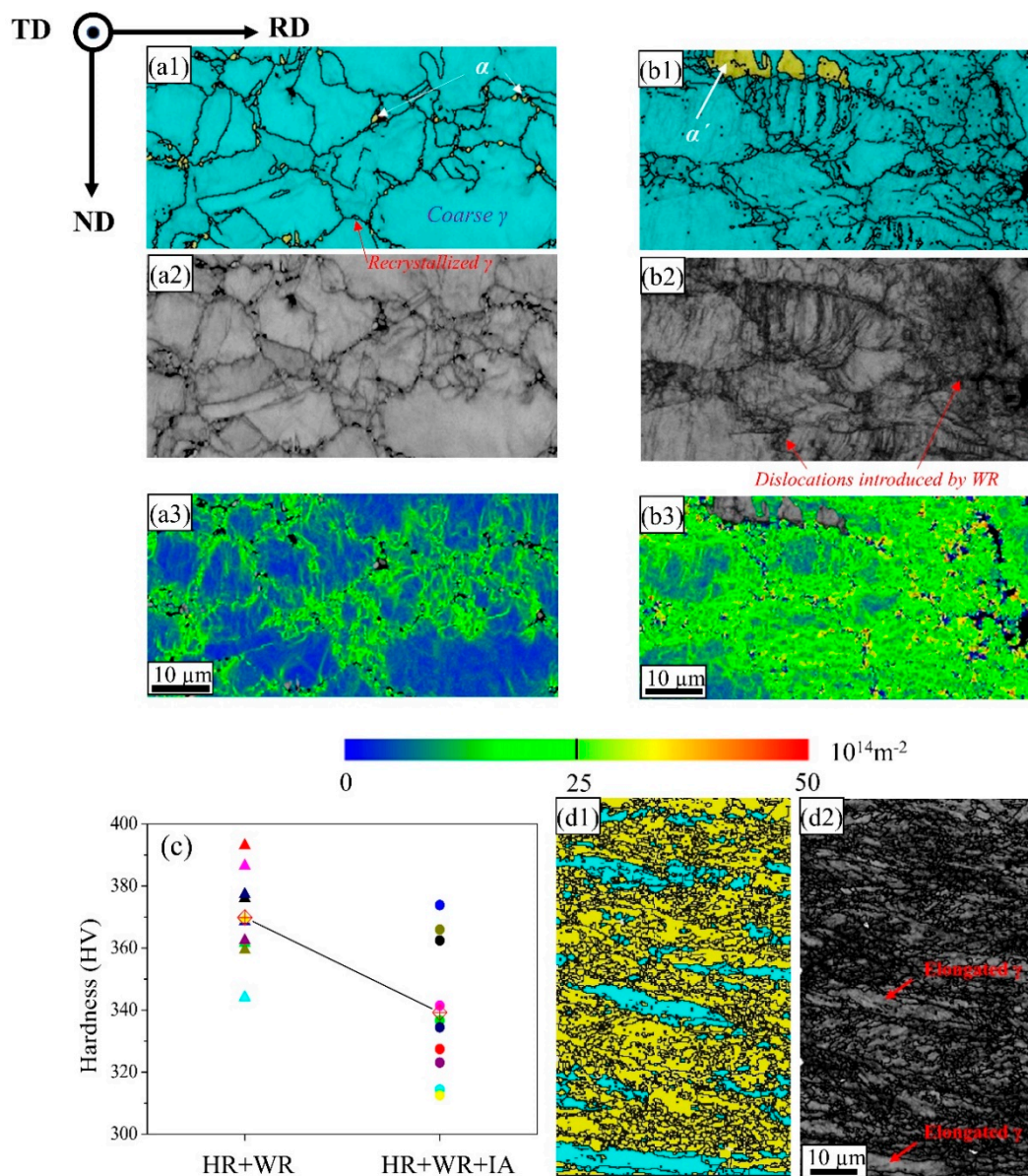


Figure 3. The microstructure of (a1,a2,a3) HR sample and (b1,b2,b3) HR+WR sample. (c) The Vickers hardness (HV) of HR+WR sample and HR+WR+IA sample. The microstructure of (d1,d2) D&P samples partitioned at 300 °C for 6 min. (a1, b1 and d1 are electron backscatter diffraction (EBSD) phase maps, wherein yellow and blue colors represent martensite/ferrite and austenite, respectively; a2, b2 and d2 are EBSD band contrast maps; a3 and b3 are the distribution of geometrically necessary dislocations (GND) densities of austenite matrix estimated based on the kernel average misorientation (KAM)). RD: Rolling direction; ND: Normal direction; TD: Transverse direction.

The dominated austenitic microstructure was maintained after warm rolling (Figure 3b1). To distinguish the difference of dislocation density between HR and HR + WR samples, the geometrically necessary dislocation (GND) densities were further estimated based on the kernel average misorientation (KAM), which represents the average misorientation between the measured point and the nearest neighbor points in the EBSD measurement (Figure 3b3). It was found that intensive dislocations were generated in austenite grains by warm rolling (Figure 3b3). Moreover, prior austenite grains were substantially elongated along the rolling direction or even fragmented into subgrains, resulting in obvious grain refinement.

The HR + WR specimen was further softened by means of intercritical annealing to facilitate subsequent deformation at room temperature. The Vickers hardness of specimens, before and after intercritical annealing, are summarized in Figure 3c. The hardness measurements were conducted in different regions through the thickness of the sample. This leads to the dispersion of hardness values due to the edge of the steel sheet which are stronger than the center resulting from warm rolling. The slight decrease of the hardness implies that some dislocations in the HR + WR specimen were annealed after IA.

Cold rolling greatly promoted the deformation-induced martensitic transformation, leading to a dual-phase lamella microstructure with austenite grains embedded in a highly dislocated martensite matrix in D&P steel (Figure 3d1,d2). The prior austenite grain boundaries (PAGB) exist before the martensitic transformation and can be retained after the formation of martensite. The martensitic matrix possesses a heterogeneous microstructure, consisting of large lenticular grains and small martensite lath. Retained austenite grains also exhibit heterogeneous morphologies and bimodal distribution. The large austenite grains with a length of 30 μm or above were elongated along the rolling direction and constituted most of the austenite phase, while fine granular austenite grains can be observed at PAGB. Abundant dislocations were introduced to the martensitic matrix by cold rolling, as showed by the low image quality of martensite phase in Figure 3d2. In contrast, it seems that the austenite grains, especially the coarse elongated ones, still contained relatively lower defects than the martensite phase (Figure 3d2).

The mechanical properties of the D&P steel processed by varying partitioning temperatures are summarized in Figure 4a. The Deformed specimen is brittle, although it possesses an ultrahigh yield strength of up to 2200 MPa. The ductility of the D&P steel was greatly enhanced after low-temperature partitioning (200 and 300 $^{\circ}\text{C}$) without a noticeable decrease of the yield strength. However, very different deformation behaviors were obtained after partitioning at a relatively high temperature (400 $^{\circ}\text{C}$). Necking was found to proceed upon yielding for the D&P400 specimen. A typical yield drop phenomenon, which is induced by the un-locking of dislocations from the interstitial C atoms [17], was observed in all specimens. It was interesting to find that Lüders deformation is also tailored by the partitioning conditions (Figure 4b). Lüders deformation dominated in D&P300 specimen and accounted for 65.5% of the total elongation. The highest ductility was obtained in D&P300 specimen, which possessed the largest Lüders strain, followed by work hardening at large plastic deformation regime (Figure 4a).

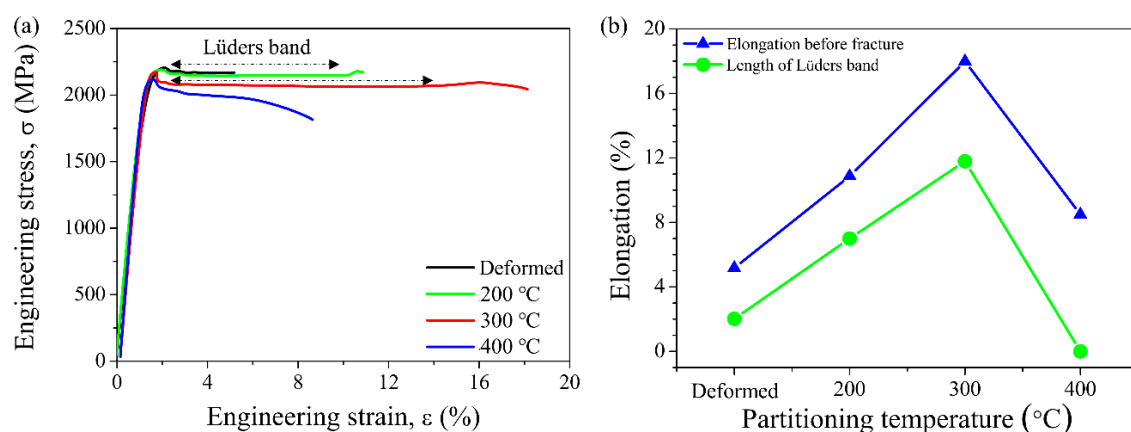


Figure 4. (a) The engineering stress–strain curves of D&P steels. (b) Effect of partitioning temperature on the ductility of D&P steels.

To understand the difference in the mechanical behaviors of various D&P specimens, 2D synchrotron X-ray diffraction measurements were carried out and the modified Williamson–Hall method was employed to study the evolution of dislocation density during the partitioning process.

2D synchrotron X-ray diffraction can provide better intensity and statistics for quantitative analysis and phase identification, especially for samples with texture, large grain size, and small quantity [18]. The broadening of diffraction peaks depends on the dislocation density (ρ), the average crystallite size (d'), and the faulting probability (β) by the following equation [14]:

$$\Delta K = 0.9/d' + (\pi A^2 b^2 / 2) \cdot \rho^{1/2} \cdot K^2 \bar{C} + \beta W_{hkl} + o(K^4 \bar{C}^2) \quad (1)$$

where $\Delta K = \cos\theta_B(\Delta 2\theta)/\lambda$ and $K = 2\sin\theta_B/\lambda$, θ_B is the diffraction angle at certain Bragg position, $\Delta 2\theta$ is the full width at half-maximum (FWHM) of the diffraction peak at θ_B , and λ is the wavelength of the X-ray. A is a constant which can be determined by the effective outer cut-off radius of dislocation, b is the Burgers vector of dislocations and W_{hkl} is the scale factor representing the peak broadening induced by a fault at exact $\{hkl\}$ deflection. Here, the faulting probability (β)-induced peak broadening was not considered because twin martensite was barely founded in the present material. \bar{C} is the average dislocation contrast factor determined by the empirical equations. Six martensite diffraction rings and four austenite diffraction rings were obtained from 2D synchrotron X-ray (Figure 5a). The 2D diffraction patterns are further converted to peak profiles to calculate ΔK and K (Figure 5b). Five martensite peaks, including (110), (200), (211), (220), and (310) were selected to calculate dislocation density of martensitic matrix. Dislocation density (ρ) and d' were subsequently determined by considering the best linear fitting between ΔK and $K^2 \bar{C}$.

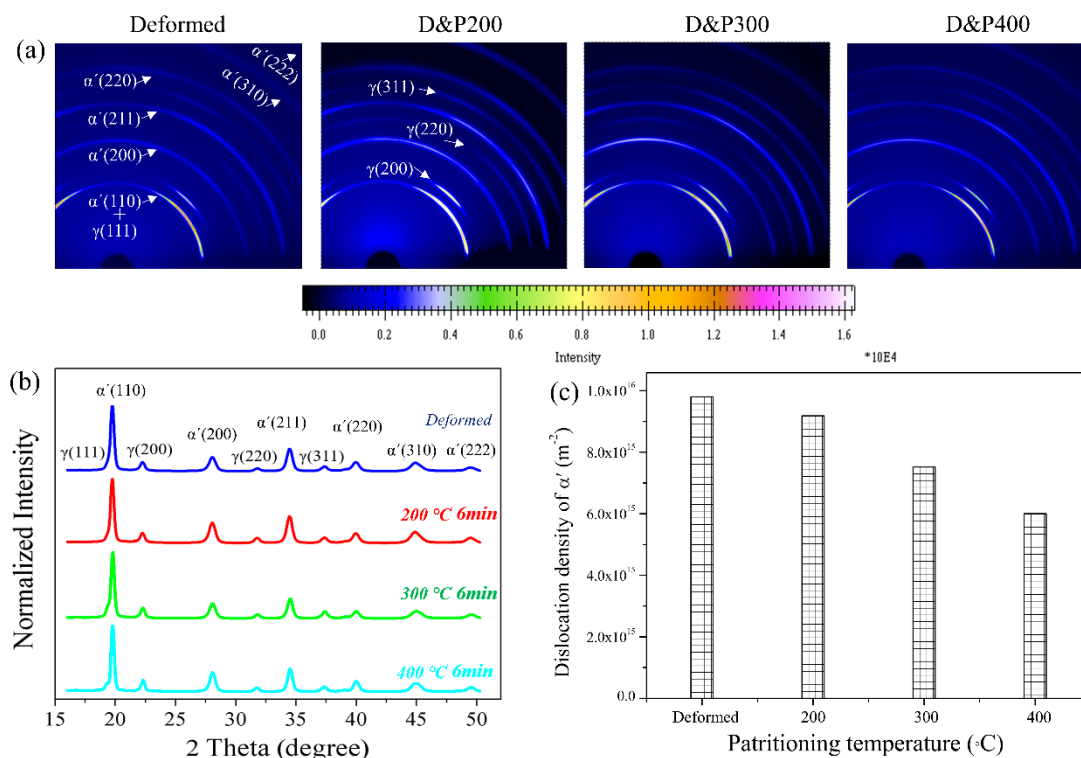


Figure 5. (a) 2D synchrotron X-ray diffraction patterns of D&P steels processed at different partitioning temperatures. Images have been colorized with high contrast to highlight the Debye diffraction rings. (b) 1D synchrotron X-ray diffraction profiles (intensity-2 theta curves) converged by 2D diffraction patterns. (c) The dislocation density of the martensitic matrix in D&P steels.

As shown in Figure 5c, the dislocation density of martensitic matrix was around 10^{16} m^{-2} after cold rolling, which is two-orders of magnitude larger than conventional thermally transformed martensite ($6 \times 10^{13} \text{ m}^{-2}$) and cold-rolled martensite ($5.39 \times 10^{14} \text{ m}^{-2}$) [19,20]. The ultrahigh dislocation density resulted from the deformation (hot rolling, warm rolling, and cold rolling) and displacive shear

deformation. The dislocation density decreased with an increase of partitioning temperature and reduced to $6 \times 10^{15} \text{ m}^{-2}$ after partitioning at 400 °C for 6 min.

4. Discussion

A heterogeneous microstructure with bimodal grain distribution was firstly developed by hot rolling (Figure 3a1). The subsequent warm rolling further enhanced the inhomogeneity and introduced intensive dislocations in austenite grains (Figure 3b1–3b3). These dislocations were slightly recovered during the intercritical annealing, while the majority can be inherited by the martensite formed during cold rolling. Note that the intercritical annealing between warm rolling and cold rolling process plays a key role in relieving the residual internal stress. Sudden cracking may take place before reaching the targeted cold rolling reduction if the HR + WR sheet is not sufficiently annealed. The amount of ferrite transformed during warm rolling and intercritical annealing were very low (Figure 2a). The sluggish transformation kinetics of ferrite was due to the high alloying contents, especially the high Mn (10%) contents, of the present steel [21]. Cold rolling enables the occurrence of deformation-induced martensitic transformation. Consequently, substantial amount of dislocations was introduced during the cold rolling process owing to the displacive shear transformation and deformation of early transformed martensite grains (Figure 3d2). In a word, although the majority of martensite was formed during cold rolling, the previous hot rolling, warm rolling, and intercritical annealing were of great importance in developing heterogeneous and dislocated microstructure in the final martensite matrix.

The partitioning process was applied to tailor the austenite stability, dislocation density, and consequently, mechanical behaviors of the D&P steel. The carbon content of austenite only increased slightly after partitioning (Figure 2b), which could be because of the formation of abundant Cottrell atmosphere, leading to a retarded carbon diffusion from martensite to austenite. These results suggest that the stability of retained austenite is not the key factor controlling the mechanical behaviors of D&P steel.

The high yield strength of D&P steels is mainly contributed by the presence of high dislocation density (Figure 4a). The contribution of the dislocation density to the yield strength can be estimated by the Taylor hardening law [11]:

$$\sigma = M\alpha\mu b \sqrt{\rho_t} \quad (2)$$

where M represents the Taylor factor and is taken as 2.9, $\alpha = 0.23$ is an empirical constant for martensite with dislocation cell structure, $\mu = 85 \text{ GPa}$ is shear modulus, and $b = 0.25 \text{ nm}$ is Burgers vector [10,11]. Therefore, the contribution of the dislocation density was estimated to be 1400, 1360, 1230, and 1100 MPa for Deformed, D&P200, D&P300, and D&P400 specimens, respectively. Therefore, the decreased yield strength of D&P400 should be around 300 MPa owing to the dislocation recovery. However, the upper yield stress of deformed sample was decreased slightly from 2204 to 2115 MPa after partitioning at 400 °C for 6 min. Therefore, other strengthening mechanisms may take place to compensate the reduction of strength caused by dislocation recovery. The reduction of dislocation density without obviously sacrificing the strength may be ascribed to the bake hardening. The carbon atoms tend to diffuse into adjacent dislocations in martensitic matrix to minimize the strain energy during the partitioning process, resulting in the formation of “Cottrell atmosphere” [17]. Dislocations surrounded by atmosphere were immobilized, leading to an increase of the upper yield stress. The increase of yield stress realized by the combination of pre-strain and strain-aging is known as bake hardening [22]. Therefore, bake hardening to some extent compensates the loss of dislocation hardening, beneficial to the high yield strength of the D&P steel. However, dislocations can break away the Cottrell atmosphere and become mobile when a sufficiently large stress is applied. This causes the occurrence of yield drop as observed in some D&P specimens (Figure 4a) [17].

The propagation of Lüders band after a yield drop depends on the work hardening ability of the specimen [23,24]. The tangled dislocation structure makes the slip of dislocation very difficult to proceed. Hence, the deformed specimen has low work hardening rate and very limited ductility

(Figure 4). After low-temperature partitioning (200 °C), D&P steel was recovered but not yet sufficiently. The D&P200 sample had improved ductility but still fractured during Lüders deformation (Figure 4). Further increasing the partitioning temperature greatly improved the ductility of samples. The D&P300 specimen showed a completed propagation of Lüders band, followed by work hardening which could be provided by the TRIP effect [10]. Although some reports on austenitic steels suggest that the TRIP effect is the reason for the propagation of Lüders band [25], it was found that the Lüders band is still present in medium Mn steels during relatively high temperature tensile deformation where the TRIP effect is completely suppressed [26]. Therefore, the TRIP-induced Lüders band mechanism is not favorable in explaining the deformation behaviors of the D&P steels with both of high dislocation density and high carbon content. The discontinuous yielding in D&P400 sample results in localized necking which is not able to propagate owing to the low work hardening ability, leading to the disappearance of Lüders deformation. This can be explained in two aspects. The annihilation of dislocation was promoted at high temperature, which greatly reduces the mobile dislocation density in the specimen. Moreover, the diffusion of interstitial carbon atoms to dislocations was energetically favored at high temperature. Namely, dislocations were more likely to be locked by carbon atoms, leading to a further reduction of the mobile dislocations. Consequently, necking proceeded quickly after the yield drop in D&P400 specimen (Figure 4).

5. Conclusions

The present work investigates the phase transformation and microstructure evolution during the D&P process. The effect of partitioning temperatures on mechanical properties of D&P steel is also addressed. The present results show that the hot rolling process can result in an initial single-phase heterogeneous microstructure. The following warm rolling is highly effective in introducing dislocations. Intercritical annealing reduces the residual stress by partially recovering dislocations, which facilitates the cold rolling at room temperature. The subsequent cold rolling enables the deformation induced martensitic transformation. Partitioning tunes the mechanical behaviors by influencing the dislocation density and austenite stability. The increase of partitioning temperature slightly changes the austenite stability because the strong interaction between dislocations and carbon atoms restricts the carbon partitioning from martensite to austenite grains. Bake hardening compensates the reduction of strength after partitioning process, enables the ultrahigh yield strength of D&P steels.

Author Contributions: M.H. proposed the project and supervised all the work. L.L. performed the experimental testing and characterization. B.H. made the material. The paper was written by L.L., B.H. and M.H.

Funding: This research was funded by the National Natural Science Foundation of China (grant number U1764252, U1560204), Research Grants Council of Hong Kong (grant number 17255016, 17203014 and 17210418), and seed fund for Basic Research of HKU (grant number 201711159029).

Acknowledgments: Authors acknowledge the experimental support from the BL14B beamline at Shanghai Synchrotron Radiation Facility, Shanghai, China.

Conflicts of Interest: The authors declare no conflict interest.

References

1. Wei, Y.; Li, Y.; Zhu, L.; Liu, Y.; Lei, X.; Wang, G.; Wu, Y.; Mi, Z.; Liu, J.; Wang, H. Evading the strength–ductility trade-off dilemma in steel through gradient hierarchical nanotwins. *Nat. Commun.* **2014**, *5*, 3580–3587. [[CrossRef](#)] [[PubMed](#)]
2. Lu, K. The future of metals. *Science* **2010**, *328*, 319–320. [[CrossRef](#)] [[PubMed](#)]
3. Li, Z.; Pradeep, K.G.; Deng, Y.; Raabe, D.; Tasan, C.C. Metastable high-entropy dual-phase alloys overcome the strength-ductility trade-off. *Nature* **2016**, *534*, 227–230. [[CrossRef](#)] [[PubMed](#)]
4. Ritchie, R.O. The conflicts between strength and toughness. *Nat. Mater.* **2011**, *10*, 817–822. [[CrossRef](#)] [[PubMed](#)]
5. Li, X.; Lu, K. Improving sustainability with simpler alloys. *Science* **2019**, *364*, 733–734. [[CrossRef](#)] [[PubMed](#)]

6. Seo, E.J.; Cho, L.; De Cooman, B.C. Application of quenching and partitioning processing to medium Mn steel. *Metall. Mater. Trans. A* **2015**, *46*, 27–31. [[CrossRef](#)]
7. Wendler, M.; Ullrich, C.; Hauser, M.; Krüger, L.; Volkova, O.; Weiß, A.; Mola, J. Quenching and partitioning (Q&P) processing of fully austenitic stainless steels. *Acta Mater.* **2017**, *133*, 346–355.
8. Mola, J.; De Cooman, B.C. Quenching and partitioning (Q&P) processing of martensitic stainless steels. *Metall. Mater. Trans. A* **2013**, *44*, 946–967.
9. Bleck, W.; Guo, X.; Ma, Y. The TRIP effect and its application in cold formable sheet steels. *Steel Res. Int.* **2017**, *88*, 1700218. [[CrossRef](#)]
10. He, B.; Hu, B.; Yen, H.; Cheng, G.; Wang, Z.; Luo, H.; Huang, M. High dislocation density-induced large ductility in deformed and partitioned steels. *Science* **2017**, *357*, 1029–1032. [[CrossRef](#)]
11. Taylor, G.I. The mechanism of plastic deformation of crystals. Part I—Theoretical. *Proc. R. Soc. London, Ser. A* **1934**, *145*, 362–387. [[CrossRef](#)]
12. Liu, L.; He, B.; Huang, M. The Role of Transformation-Induced Plasticity in the Development of Advanced High Strength Steels. *Adv. Eng. Mater.* **2018**, *20*, 1701083. [[CrossRef](#)]
13. Huang, M.; He, B. Alloy design by dislocation engineering. *J. Mater. Sci. Technol.* **2018**, *34*, 417–420. [[CrossRef](#)]
14. Ungár, T.; Ott, S.; Sanders, P.; Borbély, A.; Weertman, J. Dislocations, grain size and planar faults in nanostructured copper determined by high resolution X-ray diffraction and a new procedure of peak profile analysis. *Acta Mater.* **1998**, *46*, 3693–3699. [[CrossRef](#)]
15. Liu, L.; He, B.; Cheng, G.; Yen, H.; Huang, M. Optimum properties of quenching and partitioning steels achieved by balancing fraction and stability of retained austenite. *Scr. Mater.* **2018**, *150*, 1–6. [[CrossRef](#)]
16. Van Dijk, N.; Butt, A.; Zhao, L.; Sietsma, J.; Offerman, S.; Wright, J.; Van der Zwaag, S. Thermal stability of retained austenite in TRIP steels studied by synchrotron X-ray diffraction during cooling. *Acta Mater.* **2005**, *53*, 5439–5447. [[CrossRef](#)]
17. Cottrell, A.H.; Bilby, B. Dislocation theory of yielding and strain ageing of iron. *Proc. Phys. Soc., London, Sect. A* **1949**, *62*, 49–62. [[CrossRef](#)]
18. He, B.B.; Preckwinkel, U.; Smith, K.L. Comparison between conventional and two-dimensional XRD. *Adv. X-Ray Anal.* **2003**, *46*, 37–42.
19. Pešička, J.; Kužel, R.; Dronhofer, A.; Eggeler, G. The evolution of dislocation density during heat treatment and creep of tempered martensite ferritic steels. *Acta Mater.* **2003**, *51*, 4847–4862. [[CrossRef](#)]
20. Shintani, T.; Murata, Y. Evaluation of the dislocation density and dislocation character in cold rolled Type 304 steel determined by profile analysis of X-ray diffraction. *Acta Mater.* **2011**, *59*, 4314–4322. [[CrossRef](#)]
21. Coates, D. Diffusional growth limitation and hardenability. *Metall. Trans.* **1973**, *4*, 2313–2325. [[CrossRef](#)]
22. Soenen, B.; De, A.; Vandeputte, S.; De Cooman, B. Competition between grain boundary segregation and Cottrell atmosphere formation during static strain aging in ultra low carbon bake hardening steels. *Acta Mater.* **2004**, *52*, 3483–3492. [[CrossRef](#)]
23. Johnston, W.G. Yield points and delay times in single crystals. *J. Appl. Phys.* **1962**, *33*, 2716–2730. [[CrossRef](#)]
24. Schwab, R.; Ruff, V. On the nature of the yield point phenomenon. *Acta Mater.* **2013**, *61*, 1798–1808. [[CrossRef](#)]
25. Gao, S.; Bai, Y.; Zheng, R.; Tian, Y.; Mao, W.; Shibata, A.; Tsuji, N. Mechanism of huge Lüders-type deformation in ultrafine grained austenitic stainless steel. *Scripta Mater.* **2019**, *159*, 28–32. [[CrossRef](#)]
26. Wang, X.-G.; Huang, M.-X. Temperature dependence of Lüders strain and its correlation with martensitic transformation in a medium Mn transformation-induced plasticity steel. *J. Iron Steel Res. Int.* **2017**, *24*, 1073–1077. [[CrossRef](#)]

